Recent Enhancements to NASA's PCBoom Sonic Boom Propagation Code

Joel B. Lonzaga
NASA Langley Research Center, Hampton, Virginia 23681
Email: joel.b.lonzaga@nasa.gov

This paper presents the recent updates the author has made to PCBoom sonic boom propagation code on its computational efficiency, predictive capability, and file operations. The updated version has recently been released and has a Burgers' equation solver, which is computationally more efficient than that in the older version by 2 to 3 orders of magnitude. The updated version also enhances the accuracy of the sonic boom propagation prediction by accounting for the full wind effects on the shock wave propagation. Predictions from the updated PCBoom are compared with predictions from the older version and with data from flight tests. Other upgrades and changes that have been made in the latest version include support for Unix-like operating systems, bug fixes, and generation of new types of output files that allow for better manipulation of PCBoom-generated data.

I. Introduction

One of NASA's sonic boom propagation codes, called PCBoom, has been recently updated with improved computational efficiency and predictive capability. The updated version, recently released as PCBoom 6.7.1, has a Burgers' equation solver that is computationally more efficient than that of its predecessor, PCBoom 6.7b, by 2 to 3 orders of magnitude at the typical sampling frequencies of interest. The calculation does not use an anti-Gibbs filter, which was needed in the older version[1] to mitigate the occurrence of undesirable Gibbs oscillations. Such oscillations are artificially induced and typically arise from synthesizing a waveform having steep slopes (i.e., shocks) using Fourier synthesis. The updated version also enhances the accuracy of the prediction of sonic boom propagation by accounting for the full wind effects on the wave propagation.[2–4] This is achieved by modifying the calculation of the age parameter and the absorption coefficients to account for the Doppler shift and convective effect induced by the winds.

PCBoom was originally developed by Plotkin[5,6] as a tool for noise assessment of various military and aerospace activities involving supersonic air vehicles, and as a tool for development of

an advanced commercial supersonic transport. It originally evolved[6] from the Thomas code,[7] which is a sonic boom propagation code developed in 1972. Another code used during that era is the Hayes code, more popularly known as the ARAP code, developed by Hayes, et al.[8,9] The ARAP code uses the F-function due to Witham[10] and the nonlinear aging method (MC) developed by Middleton and Carlson[11] to numerically incorporate the nonlinear effects. Although the Thomas code employs the Thomas waveform parameter and the ratio dp/p (the ratio of overpressure to atmospheric pressure) to apply the nonlinear aging effects, the PCBoom[1] version that is managed and further developed at NASA uses the MC aging method and F-function to incorporate these effects.

The enhancement of the numerical efficiency of the NASA PCBoom is achieved by choosing the spatial step size along a ray path based on an absorption effect consideration rather than on a nonlinear one. The nonlinear-based consideration is used by the older version (PCBoom 6.7b) and most other sonic boom propagation codes.[2,12,13] In this consideration, the step size is chosen to be smaller than the shock-formation distance to avoid the situation where the waveform becomes multivalued. The shock-formation distance is inversely proportional to the maximum slope of the waveform and can be very small for strong shocks. By contrast, the current paper only considers the integrated absorption coefficients along the propagation path. The step size is chosen to be large enough such that the maximum integrated absorption coefficient is sufficiently large, but not too large to negatively impact the accuracy of the solution. The method and justification used to determine the step size is further discussed later in this paper.

Unlike the older PCBoom, the updated version accounts for the full wind effects. Although the older version already incorporated some wind effects, it uses an approximation in the calculation of the Blokhintzev amplitude factor[14–16] and age parameter[9,10,15] by replacing the ray speed with the effective sound speed. These two quantities are generally not the same; they are equal only if the propagation direction is along the direction of the wind velocity field. In the calculation of the absorption coefficients, the older version does not account at all for the motion of the medium relative to the ground, which is the reference frame used by the code. By contrast, in the updated PCBoom, the frequencies are Doppler shifted and the absorption coefficients are scaled by the wind convective index.[4] The Doppler shift is well understood as the frequency shift seen by an observer at rest with the reference frame. On the other hand, the convective index quantifies the effect with which the path length traversed by the ray through the medium differs from the path length seen by the observer.

The latest version fixes most of the known bugs in the older version and can now be run on Windows and Unix-like machines. However, the post-processors used to visualize sonic boom footprints obtained using the thin shock approximation are not yet supported on the latter operating systems. In Unix machines, the visualization can be made using a dataset written on a new type of output file. The advantage of such a dataset over that obtained using the thin shock approximation is that it accounts for the atmospheric absorption. Additionally, the latest version improves the consistency of unit specification in the input file. The altitude for the atmospheric pressure in the ATT mode for the keyword ATMOS must now be given in thousands of feet, which is the same unit as that of the altitudes for temperature, winds, and humidity.

Another key feature in the latest version is the production of a new type of output file, in addition to those generated in the older version. This file has the extension .wfm or .fpt and

provides users a greater ability to manipulate the generated data. The wfm file is generated when only one azimuthal angle around the aircraft is selected. The main data written to this file is the ground waveform that uses a ground reflection coefficient provided by the user, and that gives the time in seconds and overpressure in pounds per square foot. In addition to this waveform, it also contains information such as the ray coordinates on the ground (in feet), Steven's Perceived Loudness (PL), aircraft time, ray propagation time, azimuthal angle, run-time, and sampling frequency. On the other hand, the fpt file is generated when the full extent of the sonic boom carpet is selected. It contains the ray coordinates on the ground (longitude and latitude in degrees), PL, maximum overpressure, azimuthal angle around the aircraft, aircraft time and ray propagation time.

The remaining portion of this paper discusses in Sec. II the Burgers' equation used in the updated PCBoom to calculate the propagated waveform along a chosen ray path. The approach used to numerically solve the Burgers' equation, including that used to obtain the step size, is presented in Sec. III. An analysis of the full wind effects is made in Sec. IV to compare and contrast the updated PCBoom from the older version. Comparisons between numerical models obtained using the updated and older PCBoom as well as between numerical models and measurement are presented in Sec. V. Finally, the conclusion is given in Sec. VI.

II. Ray paths and Burgers' equation

The enhancements on the predictive capability of the updated PCBoom are achieved using a lossy Burgers' equation for sonic boom propagation along chosen propagation paths in a range-dependent, windy atmosphere. Such an equation is derived within the framework of weakly nonlinear ray theory.[2,3] In such a framework, it is assumed that the propagation is weakly nonlinear and that the medium properties vary slowly over a typical acoustic wavelength. The ray propagates along a path solely determined by linear ray theory while the acoustic energy is propagated using a nonlinear transport equation, which can be reduced to a Burgers' equation. Although the older PCBoom incorporated wind effects, it uses an approximation that leads to a substantially different solution in the presence of strong winds.

II.A. Ray path calculation

The ray paths are determined using the ray tracing equations. They are indicated by the three Cartesian components (x_1, x_2, x_3) of the ray position vector $\mathbf{x}$. In range-dependent, windy atmospheres, the ray tracing equations are the coupled differential equations[3,15]

$$\frac{d\mathbf{x}}{ds} = \frac{\mathbf{v}_o + c_o^2\mathbf{q}/\Omega}{v_r}$$

and

$$\frac{d\mathbf{q}}{ds} = -\frac{1}{v_r}\left(\frac{\Omega}{c_o}\nabla c_o + \sum_{\alpha=1}^{3} q_\alpha \nabla v_{o,\alpha}\right).$$

In these equations, s is the ray path length, c_o is the sound speed, $v_{o,\alpha}$ are the Cartesian components of the wind velocity vector $\mathbf{v}_o$, v_r is the ray speed or the magnitude of the ray velocity $\mathbf{v}_r$, q_α are the components of the slowness vector $\mathbf{q}$, and Ω is the Doppler shift induced by the wind. The ray velocity, slowness vector and Doppler shift are, respectively, given by

$$\mathbf{v}_r = c_o\hat{\mathbf{n}} + \mathbf{v}_o, \tag{1}$$

$$\mathbf{q} = \frac{\hat{\mathbf{n}}}{c_o + \mathbf{v}_o \cdot \hat{\mathbf{n}}},$$

and

$$\Omega = 1 - \mathbf{v}_o \cdot \mathbf{q}$$

where $\hat{\mathbf{n}}$ is the unit vector normal to the wavefront. The ray path length s is related to the ray propagation time t, used by the older PCBoom and in some literature, by $dt = ds/v_r$.[9,15,17]

II.B. Burgers' equation for range-dependent atmospheres

Here, we derive the Burgers' equation used in the updated PCBoom. In the derivation, we use the approximation that the nonlinear and absorption effects are both first-order effects. A consequence of this approximation is that any products involving the nonlinearity and absorption are second-order effects and are, thus, neglected. This Burgers' equation describes the evolution of the acoustic field along a ray-theoretic propagation path, and includes the full wind effects that are not treated in the older PCBoom.

For range-dependent, windy atmospheres, we use the inviscid Burgers' equation obtained by Lonzaga, et al.,[3] starting from the inviscid governing equations of fluid mechanics. A similar equation has been derived by Robinson[2] for stratified atmospheres. As is usually done in shock wave propagation, the absorption effects will be accounted for using a perturbation approach. The inviscid Burgers' equation is given by

$$\frac{\partial u}{\partial s} = \tilde{\beta} u \frac{\partial u}{\partial \tau} \tag{2}$$

where τ is the retarded time, u is a scaled acoustic pressure, and $\tilde{\beta}$ is a scaled coefficient of nonlinearity. The scaled acoustic pressure satisfies $p = p_i^{(p)} B u$ where $p = p(s,\tau)$ is the acoustic pressure, $p_i^{(p)}$ is the peak overpressure at the initial point of the ray path denoted by the subscript i, and B is the Blokhintzev scaling factor given by

$$B = \sqrt{\frac{\rho_o c_o \chi \Omega A_i}{\rho_{o,i} c_{o,i} \chi_i \Omega_i A}}. \tag{3}$$

In Eq. (3), ρ_o is the local ambient density, $\chi = c_o/v_r$, and A is the ray tube area that quantifies the spreading effect due to both the source geometry and refraction. The quantity χ has been called the convective index by the author[4] because it measures the degree to which the wind changes the speed of propagation through convection and has an important effect on the effective absorption coefficient discussed below. As with linear geometrical acoustics, the Blokhintzev factor measures

the combined effects of spreading and inhomogeneity in the medium. The scaled coefficient of nonlinearity is given by

$$\tilde{\beta} = \frac{\beta p_i^{(p)} B\Omega\chi}{\rho_o c_o^3}, \tag{4}$$

which can be viewed as an effective coefficient of nonlinearity. It has the dimensions of time/distance. Eq. (4) indicates that the influence of the nonlinearity is strong when the peak overpressure of the waveform is large.

The atmospheric absorption of sound is widely understood to be caused by classical-rotational dissipation and molecular vibrational relaxation of the gases in the atmosphere. As functions of the angular frequency ω, the classical-rotational absorption α_{cr} and the vibrational relaxation absorption coefficient α_{vr} have been modeled[2] as $\alpha_{cr}(\omega) = \omega^2 A_{cr}$ and

$$\alpha_{vr} = \sum_{\nu} \frac{A_{vr}^{(\nu)}(\omega^2\omega_\nu - i\omega^3)}{\omega^2 + \omega_\nu^2}, \tag{5}$$

respectively. In these equations, ν denotes the species of gas molecules present in the atmosphere and ω_ν is the angular vibrational frequency of the ν molecule. Both A_{cr} and $A_{vr}^{(\nu)}$ are dependent on the ambient temperature and pressure, and can be determined from Refs. [2, 18]. Using the Fourier transform pair

$$u(\mathbf{x},\tau) = \int_{-\infty}^{\infty} \frac{d\omega}{2\pi} U(\mathbf{x},\omega) e^{i\omega\tau}, \quad U(\mathbf{x},\omega) = \int_{-\infty}^{\infty} d\tau u(\mathbf{x},\tau) e^{-i\omega\tau} \tag{6}$$

of the scaled acoustic pressure, the resulting differential equation

$$\frac{dU}{ds} = -\alpha_t'(s,\omega) U(s,\omega) \tag{7}$$

due to absorption can be obtained where $\alpha_t' = \alpha_{cr} + \alpha_{vr}$ is the total absorption coefficient. Such an equation is only applicable when the medium is at rest relative to the chosen reference frame.

While Eq (2) uses the ground as the reference frame, Eq. (7) uses the propagation medium as the reference frame. The two frames of reference are not the same in the presence of wind. Consequently, we now impose the ground as the reference frame to account for wind effects in the calculation of the total absorption coefficient. Such a reference frame is used by most sonic boom propagation models including PCBoom. When the medium is moving with respect to the ground, it is necessary to apply the Doppler shift to each frequency[2,19] in Eq. (7) and use the actual path length traversed by the ray in the medium. The derivation of the full wind effects can be done using the governing equations of fluid mechanics; however, the derivation is too involved to be presented here. The final result is

$$\frac{dU}{ds} = -\alpha_t(s,\omega) U(s,\omega) \tag{8}$$

where

$$\alpha_t = \chi \alpha_t'(\Omega\omega) \tag{9}$$

is the effective absorption coefficient. To account for the presence of winds, Eq. (9) shows that 1) the frequency ω must be transformed to $\Omega\omega$ and 2) the resulting absorption coefficient must

be scaled by the convective index. While the former has been widely understood as the Doppler effect, the latter is not as widely understood. The latter's physical basis is the fact that, as seen by the observer on the ground, the wind can either compress or stretch the path length traversed by the ray through the medium. The path length is compressed when $\chi > 1$, i.e., when there is a component of the wind velocity directed opposite the acoustic propagation direction. On the other hand, the path length is stretched when $\chi < 1$. Estimates of Ω and χ are discussed in Sec. IV.C for typical jet streams.

Using a perturbation approach, Eqs. (2) and (8) can be utilized to obtain a Burgers' equation whose spectral representation is given by

$$\frac{\partial U}{\partial s} = \frac{i\omega\tilde{\beta}}{4\pi}\int_{-\infty}^{\infty} U(s,\omega')U(s,\omega-\omega')d\omega' - \alpha_t(s,\omega)U(s,\omega). \tag{10}$$

In deriving this equation, we Fourier transformed Eq. (2) using the convention shown in Eq. (6) and used the approximation that the nonlinear and absorption effects are both first-order effects. A consequence of this approximation is that any products involving the nonlinearity and absorption are second-order effects and are, thus, neglected. Although this derivation treated the nonlinear and absorption pieces separately, the same Burgers' equation would be obtained if these two pieces are treated on an equal footing from the governing equations of fluid mechanics.

III. Numerical Solution

III.A. Split-step, pseudospectral approach

There is no known analytical solution to Eq. (10). Consequently, this differential equation is typically solved using a split-step approach[1–3] where the nonlinear and absorption terms are treated separately at each spatial step. The nonlinear effects are accounted for in the time domain while the absorption effects are accounted for in the frequency domain. This approach is an approximate solution to the differential equation where the solution becomes less accurate as the step size increases.

Using the split-step, pseudospectral approach, Eq. (10) can be rewritten into two components. In the time-domain, the first component is just Eq. (2) while the second component is just Eq. (8). The advantage of this approach is that each component lends itself to an analytical solution. Using the Poisson solution,[3,20,21] the solution to Eq. (2) is

$$u(s,\tau) = u_o(\tau + u_o\Lambda(s)) \tag{11}$$

where

$$\Lambda(s) = \int_{s_o}^{s} \tilde{\beta} ds' \tag{12}$$

is the age parameter[9,15,22] defined such that it has the dimension of time, and u_o is the waveform at $s = s_o$. Similarly, the solution to Eq. (8) is

$$U(s,\omega) = U(s_o,\omega)e^{-a(s,\omega)} \tag{13}$$

where $a(s,\omega) = \int_{s_o}^{s} \alpha_t(s',\omega)ds'$ is the integrated absorption coefficient. The complete solution then involves using the analytical solution, Eq. (11), to obtain results that account for the nonlinear effects and using these results in the analytical solution, Eq. (13), to include the absorption effects.

III.B. Step size consideration

An efficiency improvement in the older PCBoom's Burgers' solver by 2-3 orders of magnitude has been achieved by employing a combination of the analytical solutions, Eqs. (11) and (13), and a spatial step size that is a compromise between numerical accuracy and computational efficiency. In the latest version, a large enough step size that does not sacrifice accuracy is chosen. This step size is generally larger than that in the older version, especially near the source.

In most modern sonic boom propagation codes,[1,2,12,13] the step size used to advance along the ray path is taken to be proportional to the propagation distance just before a shock forms. Such a shock-formation distance δs is inversely proportional to the maximum slope of the waveform in the previous step along the ray path. In a discretized waveform, this shock-formation distance is

$$\delta s \sim \Delta\tau/(\Delta p)_{max}. \tag{14}$$

For most sonic boom propagation models, this shock formation distance is converted to a propagation time by the relationship[3,17] $dt = ds/v_r$, and marching is done along the ray path with step size $\delta t = \int_{s_o}^{s} ds/v_r$. Note that v_r here is just the local sound speed if there is no wind.

The step size obtained based on Eq. (14) becomes small as $(\Delta p)_{max}$ increases. This usually happens when the peak overpressure is large, such as those of the waveforms generated by conventional aircraft. The step size is further diminished by increasing the waveform sampling rate, i.e., decreasing the time interval $\Delta\tau$. For very strong shocks and high waveform sampling rate, this step size can be very small, increasing the number of iterations to march from the initial position close to the aircraft to the final position, typically the ground.

The selection of the step size in the updated PCBoom does not consider the relationship in Eq. (14). Instead, the main consideration here is based on the integrated absorption coefficients $a(s,\omega)$ that appear in Eq. (13). If the step size at a particular step is small such that the largest value of $a(s,\omega)$ is nearly zero, then $U(s,\omega)$ would be nearly identical to $U(s_o,\omega)$. Thus, that particular step would be unproductive and can be skipped without affecting the accuracy of the solution. Consequently, here the step size is chosen such that the largest value of $a(s,\omega)$ is sufficiently large but not too large to significantly affect the accuracy. Not only does this step size increase the efficiency, it also suppresses the formation of Gibbs oscillations by ensuring that the atmospheric absorption effect is significant enough to attenuate the very high frequency components. Future work will establish a frequency and nonlinearity-dependent criterion from which the step size can be appropriately chosen.

Currently, in the updated PCBoom, there are three step settings from which the users can choose. These settings are number coded by 1, 2, and 3 that correspond to step sizes of 200, 600, and 1,000 ft, respectively. These step sizes are based on a convergence study done by the author for a low boom and a boom from a conventional aircraft. Additionally, the users are also allowed to choose the sampling rate for the waveform. However, they may not exactly get their chosen sampling rate for two reasons. First, there is a minimum number of discretized points in the waveform. Users' sampling rate that corresponds to a size below the minimum is ignored and replaced by the sampling rate that corresponds to the minimum size. Second, the final sampling rate used by the code is chosen such that it is equal to or larger than the users' sampling rate and

that the size is equal to a power of 2. The power-of-2 requirement is imposed to take advantage of the additional computational efficiency offered by some Fast Fourier Transform algorithms.

In waveforms with strong shocks, the step size used in the updated PCBoom can be larger than the shock-formation distance. In this situation, the nonlinear solution given by Eq. (11) becomes multivalued and is subsequently converted into a single-valued solution by using a procedure similar to the Middleton-Carlson method.[11] Such a procedure is based on the well-known Rankine-Hugoniot jump condition, which leads to the equal-area rule used to determine shock positions.[3,15,21]

IV. Full wind effects

IV.A. Blokhintzev amplitude scaling factor

The full solution, composed of Eqs. (11) and (13), of sonic boom propagation requires the Blokhintzev scaling factor B, which scales the overpressure and the effective coefficient of nonlinearity $\tilde{\beta}$. The form of the scaling factor used here considers the propagation effects only and follows the form used in the more recent literature.[15,21] By contrast, the form of the scaling factor used in the older PCBoom also incorporates a scalar aircraft parameter, in addition to the propagation effects. For comparison, we set aside the aircraft parameter and consider the propagation effects only. Here, the scaling factor given by Eq. (3) can be rewritten as

$$B = \sqrt{\frac{p_o c_o v_{r,i} c_{n,i} A_i}{p_{o,i} c_{o,i} v_r c_n A}} \tag{15}$$

where we have used the relations $p_o = \gamma \rho_o c_o^2$ and $\Omega = c_o/c_n$, and where

$$c_n = c_o + \mathbf{v}_o \cdot \hat{\mathbf{n}} \tag{16}$$

is the effective sound speed and γ is the ratio of the specific heats of gases in the atmosphere. By contrast, apart from the aircraft parameter, the scaling factor used in PCBoom 6.7b is identical to that given by Eq. (15) if the ray speed v_r is replaced by the effective sound speed c_n. Note that it is necessary to go into the PCBoom 6.7b source code to determine the scaling factor used by that version, as the latest technical reference[1] for that version does not explicitly show the expression for the scaling factor.

In general, the ray speed and effective sound speed are not identical. From Eq. (1), it is straightforward to show that $c_n = \mathbf{v}_r \cdot \hat{\mathbf{n}}$, i.e., the effective sound speed is the component of the ray velocity perpendicular to the wavefront. The quantities v_r and c_n are thus equal if there is no wind or if the wind velocity is parallel or antiparallel to the ray propagation. Aside from these situations, these quantities can be very different from each other.

IV.B. Age Parameter

The discrepancy in the Blokhintzev scaling factor due to propagation effects has a significant impact not only on the amplitude of the waveform but also on its distortion. The exact solution

to the inviscid Burgers' equation is given by Eq. (11), which shows that the solution is just a distortion of the waveform at the initial ray position s_o. The distortion is caused by the additive term $u_o\Lambda(s)$ to the retarded time τ. Λ is defined in Eq. (12) and has been called the age parameter due to its distortion effect. Using the expressions for $\tilde{\beta}$, χ, and Ω, the age parameter can be expressed as

$$\Lambda(s) = p_i^{(p)} \int_{s_o}^{s} \frac{\beta B \Omega \chi}{\rho_o c_o^3} ds'. \tag{17}$$

Note that the relation $dt = ds/v_r$ can be employed to express the age parameter as a function of propagation time used by the older PCBoom.

Equation (17) shows that the age parameter is dependent on the local Blokhintzev scaling factor. As with the Blokhintzev scaling factor, the age parameter in the older PCBoom is defined such that it incorporates a scalar number that describes an aircraft effect. Apart from such a proportionality constant, it can be shown that the two age parameters in the updated and older PCBoom codes are identical if there is no wind. In the presence of winds, however, these age parameters differ from each other in that the older PCBoom substitutes the effective sound speed approximation c_n for the more accurate ray speed v_r. As with the Blokhintzev scaling factor, it is necessary to go into the PCBoom 6.7b source code to definitively determine the age parameter used by the code.

IV.C. Absorption

As discussed above, the solution to Eq. (8) is given by Eq. (13) where the total absorption coefficient $\alpha_t(s,\omega)$ is

$$\alpha_t(s,\omega) = \chi\left(\Omega^2\omega^2 A_{cl} + \sum_{\nu} \frac{A_{vi}^{(\nu)}(\Omega^2\omega^2\omega_\nu - i\Omega^3\omega^3)}{\omega_\nu^2 + \Omega^2\omega^2}\right).$$

This total absorption coefficient already accounts for the full wind effects and is used in the updated PCBoom. The derivation and the physical basis of this equation are discussed in Sec. II. In contrast, the older PCBoom uses the absorption coefficient given by the same equation but with the convective index χ and Doppler shift Ω set to unity. This amounts to ignoring the effects of winds.

Ignoring the presence of wind can be a poor approximation when the wind fields are sufficiently strong. Maximum strength of typical jet streams exceeds 45 m/s, which is at least 12% of the sound speed at the altitudes where jets typically occur. At 10% of the sound speed, $\chi = \Omega \approx 0.9$ for acoustic rays propagating along the wind direction. This translates to an absorption coefficient of roughly 30% less than the absorption coefficient if there is no wind. If the acoustic rays are propagating opposite to the wind direction, the absorption coefficient is roughly 30% larger. These calculations are only approximate examples of the complexities of boom propagation. Winds are typically moving horizontally and sonic booms reaching the primary boom carpet propagate toward the ground. Additionally, the strength of jet streams typically decreases with decreasing altitude. Nevertheless, these calculations demonstrate the importance of accounting for the wind effects on the atmospheric absorption.

V. Results and Discussion

The differences in the treatment of winds between the latest and older versions of PCBoom can give rise to significantly different predicted waveforms for the same initial waveform. The predicted waveforms can be compared with each other and with a recorded signal using the peak overpressures as well as signal durations. To account for both waveform characteristics, here the unweighted sound exposure level SEL

$$\mathrm{SEL} = 10\log_{10}\left(\frac{1}{t_o p_o^2}\int_{-\infty}^{\infty} p^2(\tau)d\tau\right)$$

is used, where $t_o = 1$ s is a reference time interval and $p_o = 20$ μPa is a reference acoustic pressure. The SEL is better suited in the current application in that the purpose is to compare the predicted total acoustic energy of booms along a chosen propagation path with that of a recorded signal. The total energy comparison cannot be achieved using a noise metric that employs a weighting function or filtering method.

V.A. Comparison of numerical simulations

Here, we compare the predicted waveforms using the updated and older PCBoom versions using an N-wave generated by the Carlson F-function approximation as the initial signature. The azimuthal angle ϕ is chosen to be 0°. The aircraft is flying at a constant altitude of 50,000 ft and Mach number of 1.5 in the U.S. Standard Atmosphere. The N-wave is an approximation to the near-field signature of a conventional supersonic aircraft. Fig. 1a shows the waveforms obtained using the older PCBoom for cases with the anti-Gibbs filter turned on and off at sampling frequencies of 25.6, 51.2, and 102.4 kHz. The filter is used to suppress the formation of Gibbs oscillations, artificially induced when waveforms having steep slopes (i.e., shocks) are synthesized using Fourier analysis.

Figure 1a shows that the waveforms obtained with the anti-Gibbs filter turned off can be very different from those obtained with the filter turned on. In the waveforms obtained with the filter off represented by the dashed curves, both the peak overpressure and signal duration increase as the sampling frequency is increased. Doubling the sampling frequency results in an increase of the sound exposure level (SEL) by approximately 0.5-0.7 dB. By contrast, the waveforms obtained with the filter on, which are represented by the solid curves, do not appear to strongly depend on the sampling frequency or the step size larger than the default step size used in the older version. (Note that the default step size in that version is the shock-formation travel time multiplied by 0.05.) However, these waveforms are very different, in terms of the peak overpressure and signal duration, from those obtained with the filter off. For instance, at 102.4 kHz, the SEL of the waveform with the filter on is approximately 4 dB larger than that of the waveform without the filter. This amounts to more than doubling the total acoustic energy along the chosen ray path.

Unlike the older version, the updated PCBoom does not require an artificial smoothing filter. It only takes advantage of the absorption by the atmosphere to ensure that shocks do not form, by attenuating the very high frequency components, before the components are Fourier transformed back in the time domain. As a result of this approach, the calculated waveforms are not sensitive to

the sampling frequency (above the required minimum) or the step size chosen by the users. Three waveforms, which are nearly identical, are plotted in Fig. 1b. They are obtained using the updated PCBoom using the step size code 2 (see Sec. III.B) and correspond to sampling frequencies of 34.3, 68.7, and 137.4 kHz. The waveforms nearly overlap with each other resulting in SELs that only differ by a few hundredths of a dB as the sampling frequency is doubled.

One way to assess the performance of the two PCBoom versions is to compare the waveforms generated by the two codes. Fig. 2 shows two such waveforms generated by the updated and older versions using the US Standard Atmosphere. These waveforms are two of those already plotted in Fig. 1. The sampling frequency is 137.4 kHz for the waveform generated by the updated version and 102.4 kHz for that generated by the older version. Note that the sampling frequency in the updated PCBoom cannot be entirely prescribed as it is dependent on the requirement that the size of the waveform is a power of 2 (see Sec. III.B). The peak overpressure and signal duration of the first waveform are slightly larger than those of the second. Additionally, the first waveform has a SEL that is approximately 0.5 dB larger than that of the second waveform. Since these calculations use a windless atmosphere, the significant differences in the results can't be attributed to the differences in the approximations used to account for the wind effects. Neither can they be attributed to the step size used in either version for reasons already discussed in the previous two paragraphs. It is likely, though, that the occurrence of the Gibbs oscillations in the older version and the use of the filter to remove such numerical artifacts have contributed to such differences, resulting in the older PCBoom being less representative of realistic sonic boom propagation than the updated version.

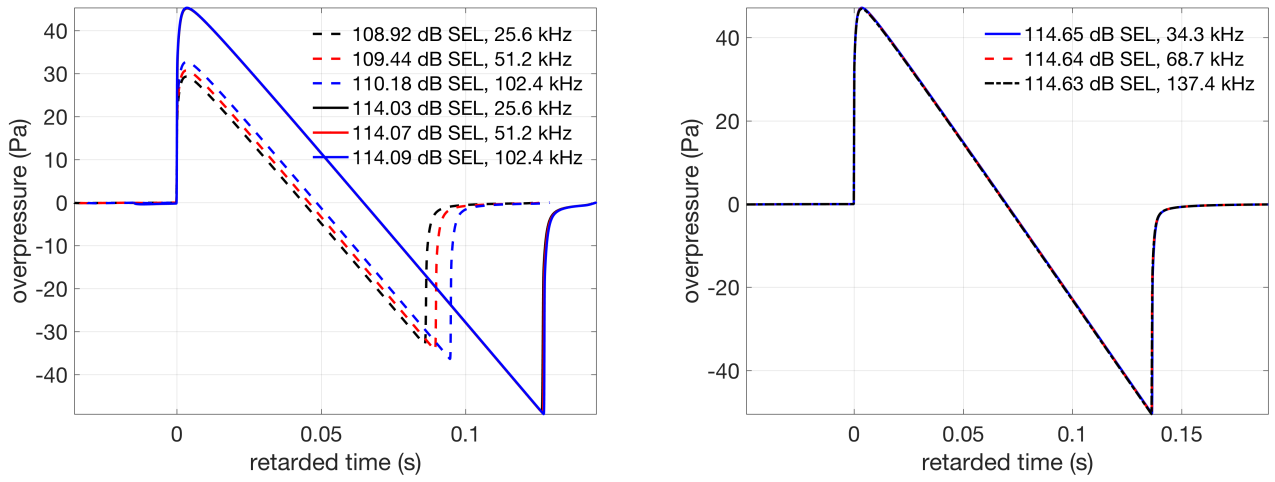

Figure 1: Comparison of predicted ground waveforms using PCBoom 6.7b (a) and PCBoom 6.7.1 (b). The waveforms in (a) are for cases with an anti-Gibbs filter turned off represented by the dashed curves and with the filter turned on shown by the solid curves. The atmosphere used is the US. Standard Atmosphere and the initial signature is an N-wave that approximates the near-field conventional aircraft signature.

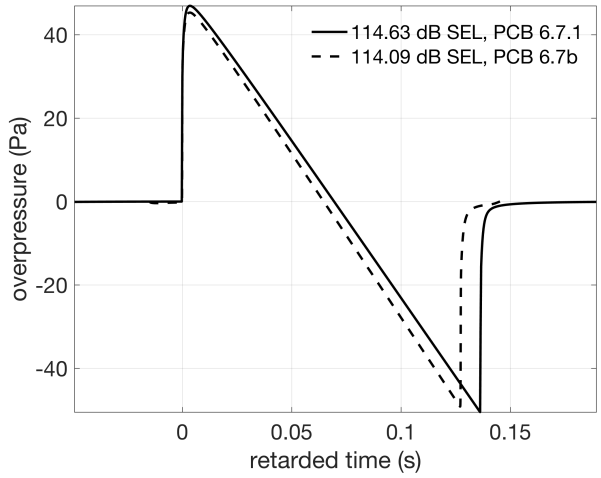

Figure 2: Comparison of predicted ground waveforms using the updated (PCBoom 6.7.1) and older (PCBoom 6.7b) versions of PCBoom. The atmosphere used is the US. Standard Atmosphere and the initial signature is an N-wave that approximates the near-field conventional aircraft signature.

V.B. Comparison of computational efficiency

Another way to assess the performance of the two PCBoom versions is to compare their computational efficiencies. For this study, a Windows Operating System (OS) is used since the older PCBoom runs only on this OS. This Windows system, however, is running on a VMWare Fusion virtual machine installed in a 2015 MacBook running MacOS X. While the MacBook has a 2.5 GHz Intel Core i7 processor and 16-GB memory, the virtual machine is only allotted 4 processor cores and 4-GB memory.

Figure 3a shows the average runtimes for the older PCBoom for cases with and without the anti-Gibbs filter. These cases are the same as those discussed in Sec. V.A where three different sampling frequencies are employed. Although the use of the filter reduces the runtimes, the runtimes even with the filter on are too large for practical uses. At the typical sampling frequency of 51.2 kHz, the average runtime with the filter on is in excess of 130 s. This runtime increases quadratically with sampling frequency and appears to be even larger for cases such as those shown in Fig. 5 with complicated initial signatures.

By contrast, the average runtime for the updated PCBoom is shown in Fig. 3b for the same cases discussed in Sec. V.A. The average runtime is about 0.2 s at a sampling frequency of 68 kHz for the same propagation conditions considered by the older version. The runtime at the typical sampling frequency of 51.2 kHz can be interpolated to be about 0.16 s. At this sampling frequency, the ratio of the runtime for the older PCBoom to that of the updated version is in excess of 800. In general, the ratio for different sampling frequencies is shown in Fig. 4, from which we conclude that the updated PCBoom is faster than the older version by 2-3 orders of magnitude at the typical sampling frequencies of interest and for the propagation cases investigated here.

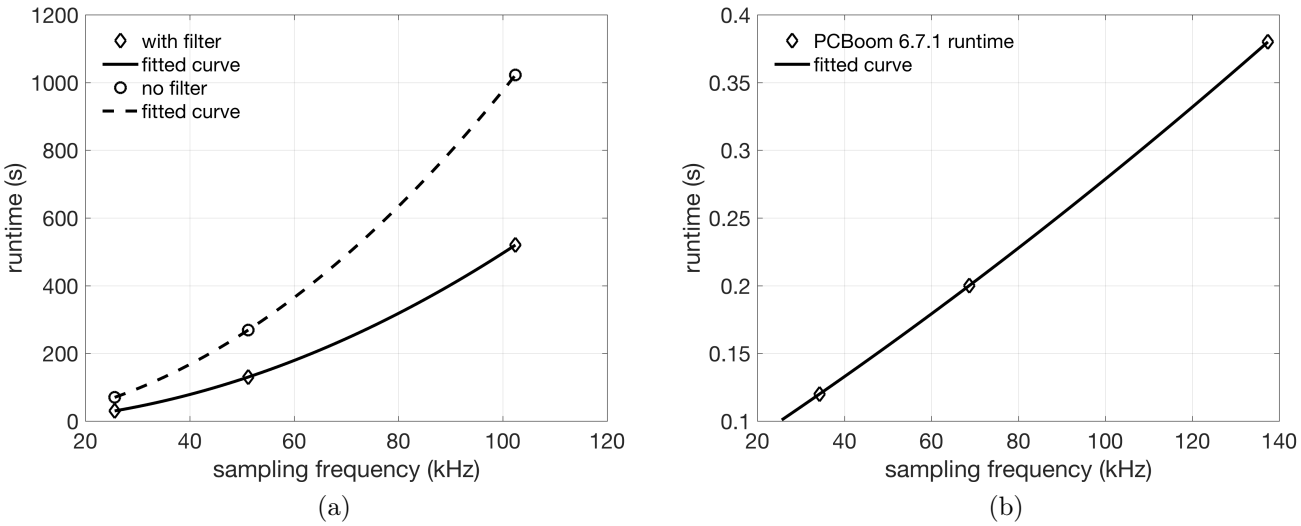

Figure 3: Runtimes for the older (a) and updated (b) versions of PCBoom. These runtimes correspond to the waveforms presented in Fig. 1.

V.C. Comparison due to wind effects

In Sec. V.A, it was discussed how the anti-Gibbs filtering impacts the solutions from the older PCBoom. Here, it is necessary to minimize these numerical artifacts to fully focus on the comparison due to the wind effects. As a result, a notional boom with low initial peak overpressure is utilized. Such a boom, a result of the Lockheed Martin N+2 design (LM-N2),[23] is propagated through the US Standard Atmosphere using both updated and older PCBoom versions. The ground waveforms are plotted in Fig. 5a. The waveforms almost overlap with each other and the SELs only differ by a few hundredths of a dB. Since the anti-Gibbs filter is used in the older version, this comparison demonstrates that use of the filter does not affect the results from the older version in cases with low initial peak overpressures.

The result that both PCBoom versions produce almost identical waveforms is rather remarkable. It is especially so given the large discrepancy between the waveforms obtained for the cases using a conventional aircraft discussed in Sec. V.A. Such a result for the LM-N2 case can likely be attributed to the initial peak overpressure being small. The conventional aircraft's initial waveform has a peak overpressure of about 500 Pa, while the LM-N2 initial waveform is about a third of that. The smaller peak overpressure in the latter waveform prevents the waveform from completely transforming into an N-wave. This is supported by the plots in Fig. 5a where strong shocks, characterized by both small rise time and large pressure difference, are not present. Development of strong shocks is a nonlinear effect and is encapsulated by the effective coefficient of nonlinearity $\tilde{\beta}^3$ given by Eq. (4). In addition to being proportional to the initial peak overpressure, $\tilde{\beta}$ is also responsible for the distortion of the waveform through the age parameter, which is just the integrated $\tilde{\beta}$ along the ray path, as given by Eq. (12). It takes a large peak overpressure for the corresponding portion of the waveform to travel faster than, and catch up with, the leading portion of the boom.

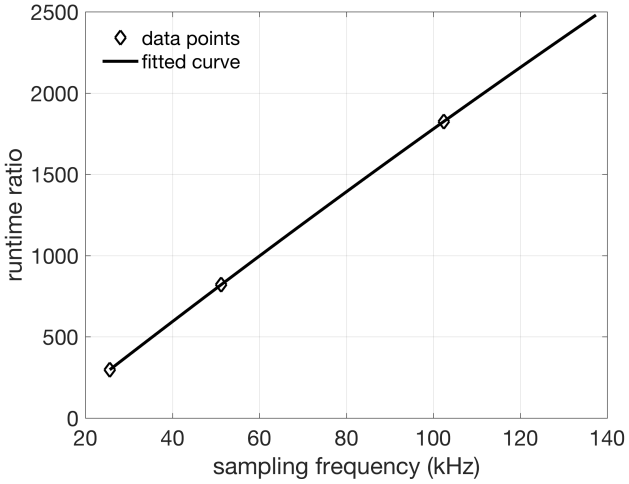

Figure 4: Ratio of the runtimes for the older version to the runtimes of the updated version of PCBoom. The individual runtimes were taken from those shown in Fig. 3.

Having minimized the impact of the numerical artifacts on our comparison by using the LM-N2 low boom as the initial signature, we can now investigate the full wind effects using the same low boom signatures. Fig. 5b shows a comparison between the waveforms generated by the PCBoom versions. For this comparison, there is a tail wind and a component of wind blowing along the direction of the chosen acoustic ray. This wind component reduces not only the effective absorption coefficient but also the effective coefficient of nonlinearity. As shown in Sec. II, the effective coefficient of nonlinearity $\tilde{\beta}$ increases with the Doppler shift Ω and with the convective index χ. However, both Ω and χ in this situation are less than unity because there is a component of wind blowing along the ray propagation direction. Since the wind direction is not exactly along the ray propagation, then the ray speed v_r and the effective sound speed c_n are not equal, as discussed in Sec. IV.A. Consequently, the effective nonlinear coefficient used in the updated version is smaller than that used in the older version. This then explains the plots shown in Fig. 5b where the waveform generated by the updated version has a larger peak overpressure but shorter signal duration compared to the waveform generated by the older version.

V.D. Comparison of models with data from flight tests

1. SonicBAT Flight Test

In this section, results from the updated and older PCBoom versions are compared with a waveform recorded by a microphone mounted at a wingtip of a TG-14 glider. The recording was made from the flight 6 pass 2 event during NASA's Sonic Booms in Atmospheric Turbulence (SonicBAT) overflight campaign[24] at the Edwards Air Force Base (EAFB) in 2016. The event was generated by a conventional aircraft flying at an altitude of 34,200 ft above sea level with a nearly constant supersonic speed at a Mach number of 1.38. During the passage of the boom, the TG-14 was gliding at a height of approximately 7,400 ft with a nearly horizontal velocity of 104 ft/s.

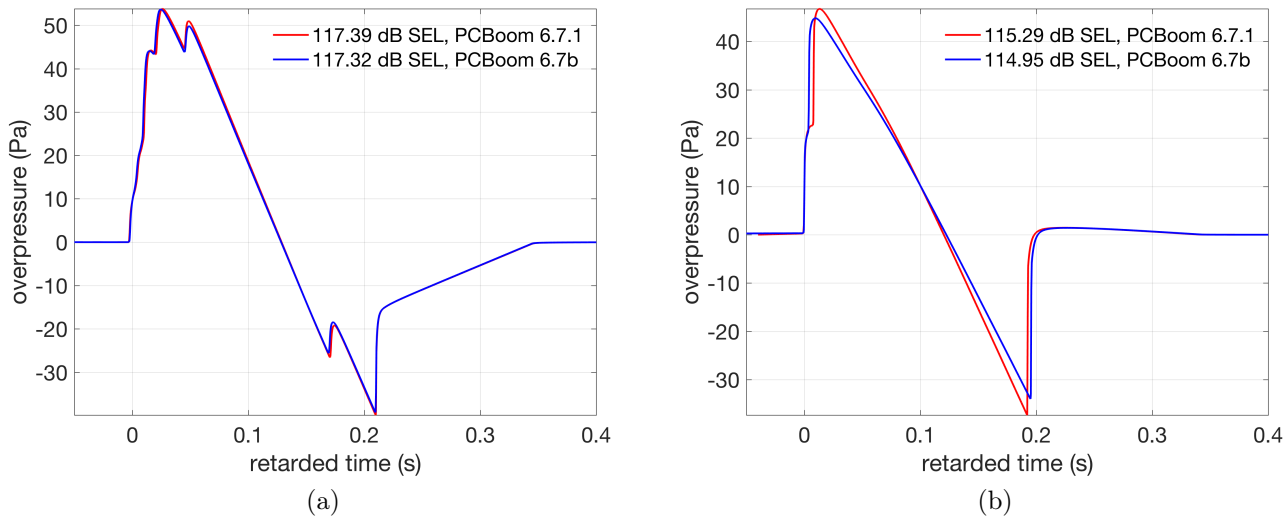

Figure 5: Comparison of ground waveforms from a near-field, low-boom signature propagated using both PCBoom 6.7b and 6.7.1 using the U.S Standard Atmosphere (a) and a realistic atmosphere with moderate winds (b).

The recorded waveform, presented in Fig. 6, is compared with the waveforms calculated using the updated and older PCBoom versions. Because the glider was moving relative to PCBoom's reference frame, the ground, the recorded waveform is Doppler shifted to allow for comparison with the predicted waveform. The Doppler shift decreases (increases) the signal duration if the glider had a velocity component that was along (opposite to) the propagation direction of the recorded boom. In the figure, the predicted waveforms are each calculated from the same initial aircraft signature. The initial signature is an N-wave approximation to the actual but complicated aircraft signature, and is obtained using PCBoom's built-in Carlson F-function.[1] The aircraft signature is then propagated through the atmosphere whose conditions were measured during the flight using a weather balloon.

Based on Fig. 6, each predicted waveform is different from the Doppler-shifted recorded signal. However, the waveform calculated using the older PCBoom has a larger discrepancy from the recorded signal than does the waveform obtained using the updated version. The former has a SEL that is approximately 2 dB smaller than that of the measured signal. By contrast, the SEL of the waveform generated by the updated PCBoom is only about 1 dB smaller. This finding appears to support our previous observation that the older PCBoom tends to yield waveforms with reduced peak overpressures and signal durations compared to those of the waveforms obtained using the updated version.

The recorded signal is also compared with a prediction, shown in Fig. 7a, calculated using a computational fluid dynamics (CFD) near-field solution as the initial signature depicted in Fig. 7b. The near-field solution is drawn from the CFD solution dataset provided by The Boeing Company.[25] The prediction is made using the updated PCBoom only, as the Burgers' solver in the older version consistently breaks down at runtime. The runtime error appears to be caused by the existence of the compression phases after the first transition from compression to expansion.

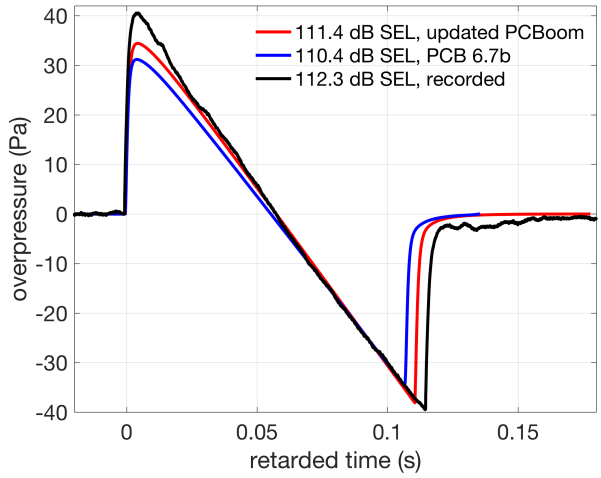

Figure 6: Comparison of predicted waveforms with a recorded signal from an event during the SonicBAT Flight Test in EAFB. The models use the same initial signature generated by the PCBoom's built-in Carlson F-function approximation.

The transition is located at the aircraft axis of approximately 35 ft (see Fig. 7b). When such compression phases are removed (i.e., $dp/p = 0$), the older Burgers' solver was able to finish the calculation.

The comparison between the recorded signal and the predicted waveform is shown in Fig. 7a, from which the peak overpressure and signal duration of the predicted waveform are seen to be nearly identical to those of the recorded signal. Although the curves in the two waveforms connecting the phase during maximum compression and the phase during maximum expansion do not exactly match, the SELs of the waveforms only differ from each other by a few hundredths of a dB. Additional recorded signals are available from SonicBAT test. A more complete comparison between predicted and recorded waveforms will be the subject of future work.

2. QSF 2018

In addition to the waveform, a predicted sonic boom carpet edge can also be compared with measurement. Fig. 8 shows the locations of the microphones (red circles in Fig. 8a and black squares in Fig. 8b) deployed during the Quiet Supersonic Flight Test in November 2018 (QSF18) conducted in and around Galveston, Texas. The quiet or low booms were generated by special dive maneuvers performed by conventional aircraft. Using the as-flown flight trajectory and the weather conditions measured by a weather balloon, the total area on the ground ensonified by the the boom, called the boom carpet, can be estimated. Fig. 8a shows the predicted boom carpet for the flight 4 pass 1 event. The red to blue dots are acoustic rays that intersect with either the ground or water. Those at the outermost, down-track portion of the boom carpet determine the carpet edge, beyond which acoustics rays are refracted upward and never intersect with the ground or water.

The boom carpet shown in Fig. 8a is generated by the updated version of PCBoom. Based on

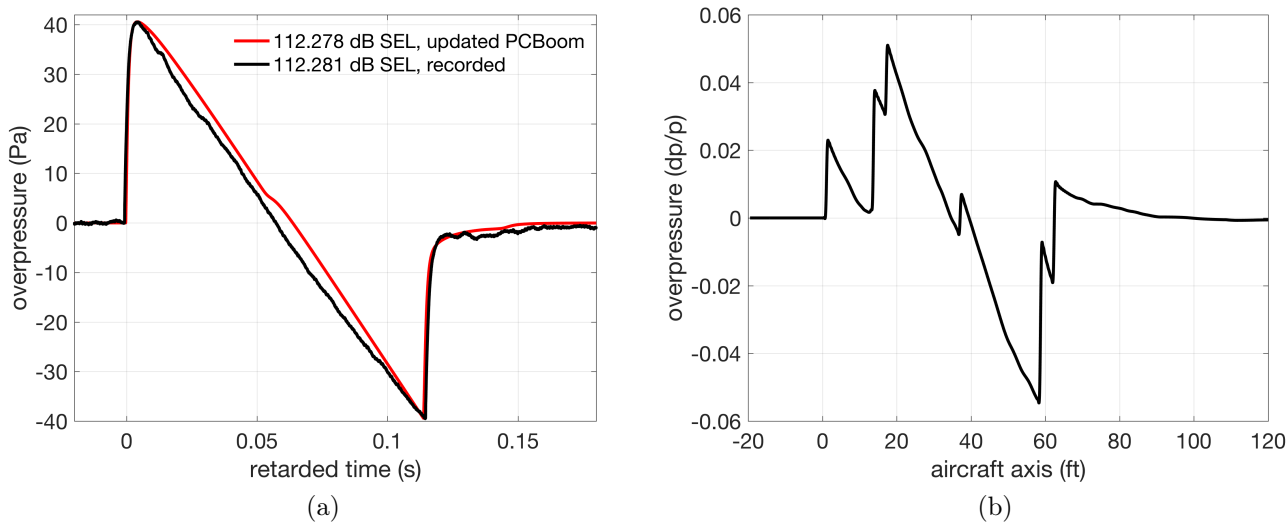

(a) (b)

Figure 7: Comparison of a predicted waveform with a recorded signal (a) from an event during the SonicBAT Flight Test in EAFB using an initial signature (b) generated using a CFD solution.

this figure, this version predicts that the microphones labeled D and F, for Delta and Foxtrot, are well within the boom carpet and are thus ensonified by the boom. By contrast, the boom carpet shown in Fig. 8b is obtained using the older PCBoom. From this figure, microphones D and F are predicted to be outside the carpet and should not have recorded the boom during this event. The recordings from these microphones, however, show that these microphones were indeed ensonified by the boom. Based on the comparison made for this event and for several other events during QSF18, the updated version appears to be more accurate than the older version in predicting the edge of the carpet.

The Schulflat mode was used in the updated PCBoom to generate the carpet shown in Fig. 8a. Although this mode is already present in the older version, this mode appears to be nonfunctional in that version due to a runtime error in one of the post processors when the Schulflat mode is selected. The runtime error is specifically true for the cases used by the author and appears to be caused by some formatting issues. Additionally, the Schulflat mode has been further enhanced in the updated PCBoom to better predict the width and edge of the carpet. Such an enhancement can shift the carpet edge by a few miles.

Because calculation of the solution to the Burgers' equation in the older version is very inefficient and time consuming, boom carpets have previously been visualized only in terms of the maximum overpressure obtained using the thin shock approximation. This solution neither uses the Burgers' equation nor accounts for the losses due to the atmospheric absorption. However, the carpet of a full flight envelope with denser ray points on the ground can now be made with the development of the fast Burgers' solution in the updated PCBoom that accounts for the atmospheric absorption. In addition to the maximum overpressure, this footprint can also be visualized in terms of additional metrics such as the Stevens' Perceived Loudness.

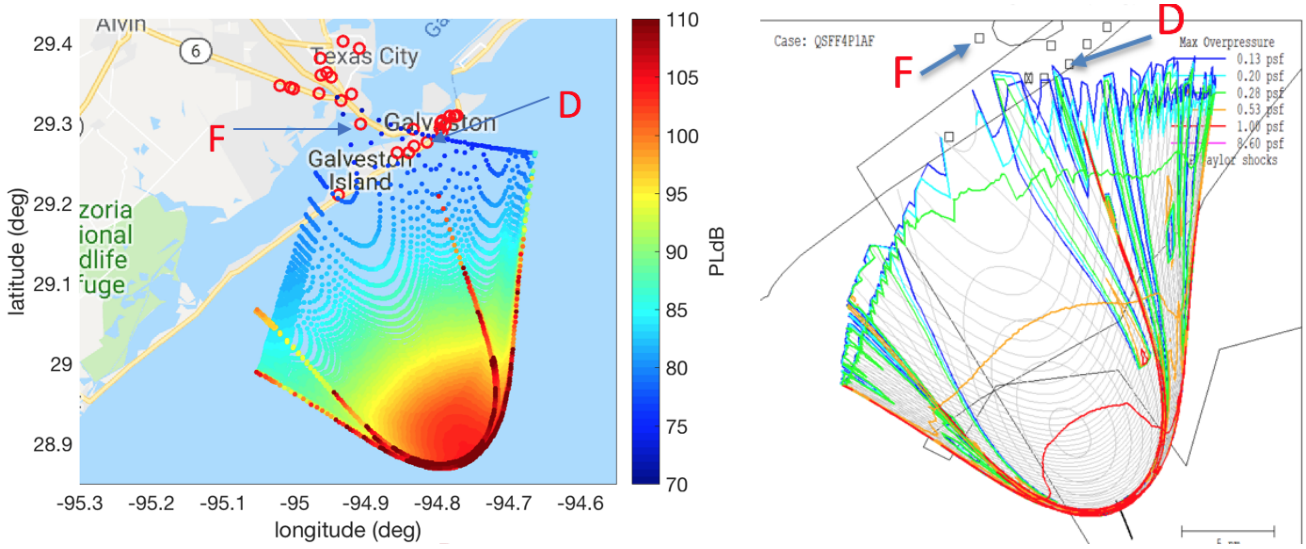

(a) (b)

Figure 8: Comparison of boom carpet predictions using the updated (a) and the older (b) PCBoom versions for the Flight 4 Pass 1 event during QSF18. The accuracy of the carpet edge predictions is determined by the recordings of the microphones deployed during the flight test.

VI. Conclusions

This paper discussed recent enhancements to NASA's PCBoom propagation code. The enhancements can be categorized into numerical and physics-based. The numerical enhancements have greatly improved the speed of the Burgers' equation solver by 2-3 orders of magnitude. The increase in the computational efficiency is achieved through a methodology of step size selection that is absorption effect-based rather than nonlinear effect-based, used by the older PCBoom version and other sonic boom propagation codes. With such a methodology, the undesirable Gibbs oscillations are automatically suppressed by a step size that allows the actual atmospheric absorption to attenuate the high-frequency components of the signal. By contrast, the nonlinear-based consideration relies heavily on the shock-formation distance to determine the step size, which can be very small for strong shocks.

The physics-based enhancements were primarily focused on incorporating the full wind effects into the calculation of the Blokhintzev scaling factor, age parameter, and atmospheric absorption coefficients. It has been previously shown, based on a derivation from the governing equations of fluid mechanics, that the scaling factor and the age parameter are both dependent on the magnitude of the ray velocity v_r. The older version, however, uses the effective sound speed that approximates v_r. These two quantities are generally not the same. The difference is large for strong winds and increases when the wind velocity becomes more and more perpendicular to the propagation direction.

The atmospheric absorption coefficients were also enhanced by incorporating the Doppler shift and convective effect of winds. The older version uses absorption coefficients that are calculated under the assumption that the medium is at rest relative to the ground, which is the code's frame

of reference. To account for the motion of the medium in the updated PCBoom, the frequencies were Doppler shifted and the integrating path length was scaled according to the convective effect of the winds.

The numerical models obtained using the older and updated versions of PCBoom were compared to measured data from SonicBAT and from the Quiet Supersonic Flight Test. The models from the updated version agree with the measurement much better than those obtained from the older PCBoom.

Acknowledgement

The author would like to acknowledge Dr. Randoph H. Cabell of the Structural Acoustics Branch at NASA Langley for his valuable comments and suggestions that have led to the improvement of this manuscript. The author would also like to acknowledge The Boeing Company and the FAA for access to the CFD data afforded to NASA. This work was supported by the NASA Advanced Air Vehicles Program, Commercial Supersonic Technology Project.

References

[1]Page, J. A., Plotkin, K. J., and Wilmer, C., "PCBoom Version 6.6 Technical Reference and User Manual," Tech. Rep., WYLE LABORATORIES, INC., 2010.

[2]Robinson, L. D., *Sonic boom propagation through an inhomogeneous, windy atmosphere*, Ph.D. Thesis, The University of Texas at Austin, 1991.

[3]Lonzaga, J. B., Waxler, R. M., Assink, J. D., and Talmadge, C. L., "Modelling waveforms of infrasound arrivals from impulsive sources using weakly non-linear ray theory," *Geophysical Journal International*, Vol. 200, No. 3, 2015, pp. 1347–1361.

[4]Lonzaga, J. B., "Time-domain modeling of the wind effects on the nonlinearity and absorption of sonic booms," *The Journal of the Acoustical Society of America*, Vol. 143, No. 3, 2018, pp. 1914–1914.

[5]Plotkin, K. J., "Pcboom3 sonic boom prediction model-version 1.0 c," Tech. Rep., WYLE RESEARCH LAB ARLINGTON VA, 1996.

[6]Plotkin, K. J., "State of the art of sonic boom modeling," *The Journal of the Acoustical Society of America*, Vol. 111, No. 1, 2002, pp. 530–536.

[7]Thomas, C. L., "Extrapolation of sonic boom pressure signatures by the waveform parameter method," Tech. Rep., NASA TN D-6832, 1972.

[8]Hayes, W. D., Haefeli, R. C., and Kulsrud, H. E., "Sonic boom propagation in a stratified atmosphere, with computer program," Tech. Rep., NASA CR-1299, 1969.

[9]Hayes, W. D. and Runyan Jr, H. L., "Sonic-boom propagation through a stratified atmosphere," *The Journal of the Acoustical Society of America*, Vol. 51, 1972, pp. 695–701.

[10]Whitham, G. B., "The flow pattern of a supersonic projectile," *Communications on pure and applied mathematics*, Vol. 5, No. 3, 1952, pp. 301–348.

[11]Middleton, W. D. and Carlson, H. W., "A numerical method for calculating near-field sonic-boom pressure signatures," Tech. Rep., NASA TN D-6832, 1965.

[12]Cleveland, R. O., Hamilton, M. F., and Blackstock, D. T., "Time-domain modeling of finite-amplitude sound in relaxing fluids," *The Journal of the Acoustical Society of America*, Vol. 99, No. 6, 1996, pp. 3312–3318.

[13]Rallabhandi, S. K., "Advanced sonic boom prediction using the augmented Burgers equation," *Journal of Aircraft*, Vol. 48, No. 4, 2011, pp. 1245–1253.

[14]Blokhintzev, D., "The propagation of sound in an inhomogeneous and moving medium I," *The Journal of the Acoustical Society of America*, Vol. 18, No. 2, 1946, pp. 322–328.

[15]Pierce, A., *Acoustics: An Introduction to Its Physical Principles and Applications*, Acoustical Society of America, revised edition ed., 1989.

[16]Maglieri, D. J., Bobbitt, P. J., Plotkin, K. J., Shepherd, K. P., Coen, P. G., and Richwine, D. M., "Sonic boom: Six decades of research," Tech. Rep., NASA/SP-2014-622, 2014.

[17]Brekhovskikh, L. M. and Godin, O. A., *Acoustics of layered media II: point sources and bounded beams*, Vol. 10, Springer Science & Business Media, 2013.

[18]Bass, H. E., Sutherland, L. C., Zuckerwar, A. J., Blackstock, D. T., and Hester, D., "Atmospheric absorption of sound: Further developments," *The Journal of the Acoustical Society of America*, Vol. 97, No. 1, 1995, pp. 680–683.

[19]Salamone, J. and Sparrow, V. W., "A sonic boom propagation model including mean flow atmospheric effects," *AIP Conference Proceedings*, Vol. 1474, AIP, 2012, pp. 311–318.

[20]Landau, L. and Lifshitz, E., *Fluid Mechanics*, Vol. 6, Elsevier Butterworth Heinemann, 2nd ed., 1987.

[21]Hamilton, M. and Blackstock, D., *Nonlinear Acoustics*, Acoustical Society of America, 2008.

[22]Whitham, G. B., "The propagation of weak spherical shocks in stars," *Communications on Pure and Applied Mathematics*, Vol. 6, No. 3, 1953, pp. 397–414.

[23]Morgenstern, J., Norstrud, N., Sokhey, J., Martens, S., and Alonso, J. J., "Advanced concept studies for supersonic commercial transports entering service in the 2018 to 2020 period," Tech. Rep., Lockheed Martin Corporation, 2013.

[24]Hobbs, C. and Bradley, K., "Atmospheric turbulence effects on sonic boom signatures," *The Journal of the Acoustical Society of America*, Vol. 143, No. 3, 2018, pp. 1912–1912.

[25]Shen, H., Ladd, J., and Michal, T., "F/A-18B sonic boom near-field CFD for FAA - in support of SSTG procedures subgroup efforts," The International Civil Aviation Organization, CAEP WG1 Meeting, Sept. 2018.